Cesium based Polyoxometalates as co-catalysts for Proton Exchange Membrane Fuel Cells (PEMFC)

Gianluca D'Angelo
Instituto Superior Técnico, Universidade Técnica de Lisboa

Abstract. This work was oriented on the synthesis and characterization of catalytic supports of PEM-Fuel cells based on polyoxometalates (POM) containing Cesium ($Cs_xH_{5-x}PMo_{10}V_2O_{40}\cdot 8H_2O$), starting from the heteropolyacid $H_5PMo_{10}V_2O_{40}\cdot 8H_2O$. Three POM with a different amount of Cesium were synthesized and analyzed, respectively: $Cs_{2.5}H_{2.5}PMo_{10}V_2O_{40}\cdot 8H_2O$, $Cs_3H_2PMo_{10}V_2O_{40}\cdot 8H_2O$ and $Cs_{3.5}H_{1.5}PMo_{10}V_2O_{40}\cdot 8H_2O$. Once synthesized, in order to obtain information on the morphology and composition, the compounds were analyzed with physical analysis (SEM-XRD, IR, XRD). Afterwards inks were prepared and underwent electrochemical characterizations, using the three synthetized POMs and two different platinum contents. Three types of analysis were performed: cyclic voltammetry (CV) in order to characterize the redox processes of the investigated samples; liner sweep voltammetry (LSV) with rotating disk electrode (RRDE) in order to study the kinetics of the oxygen reduction reaction (ORR), and finally the CO-stripping in order to obtain information on catalyst poisoning by CO. Moreover, tests have been performed in a complete fuel cell, recording polarization curves and electrochemical impedance spectroscopy. The good results open promising future developments in the use of this type of technology.

Key words: Catalysis, Oxygen Reduction Reaction, Polyoxometalates, PEM fuel cells, Reduced platinum loading.

1. Introduction

Polymer electrolyte membrane (PEM) fuel cells are promising candidates for mobile applications (e.g. cars) due to the low operating temperature that allows a relatively short start-up, no toxic emission and fairly good performance. Unfortunately the current high costs, mainly related to the use of noble metals as catalysts and of perfluorosulphonated membranes, still remain a big limitation for the commercialization of this technology. PEMFCs are particularly amenable for use as a laboratory experiment, due to safety and operational advantages[1], where the lifetime requirements and the high loadings of noble metals for mobile applications can be achieved. Carbon supported Pt nanoparticles are by far the most used catalyst for oxygen reduction (ORR) and hydrogen oxidation (HOR) in PEMFC[2]. The use of noble metals, and mainly of Pt, is necessary because the ORR needs a very efficient catalysis for the cleavage of O=O bond[3]. Due to the high value of the platinum, in the path towards fuel cells commercialization, one of the big challenges is to reduce the catalyst material cost. Two approaches are currently very attractive: the exploration of non-noble catalysts and the reduction of the Pt loading[4]. In the last years,

the research is focused on the development of compounds that make it possible to reduce the amount of Platinum, as heteropolyacids (HPAs). Thanks to their acidity and porosity, HPA, provide a high proton concentration on catalytic sites, and avoid the aggregation of catalytic particles during the fuel cell operation. Heteropolyacids of Keggin type structure are very relevant because they can adsorb Pt nanoparticles; unfortunately due to their high water solubility they are prone to lose rapidly catalytic activity[2]. In order to increase the water solubility, insoluble heteropolyacids salts are prepared by partly exchanging protons with larger cations (Cs^+ in this paper). Polyoxometalates (POMs) are a class of inorganic compounds that is unmatched not only in terms of molecular and electronic structural versatility, but in terms of also regarding reactivity and relevance to analytical chemistry, catalysis, biology, medicine, geochemistry, materials science and topology[5]. Molybdovanadophosphoric acid ($H_{3+x}PMo_{12-x}V_xO_{40}$), has been found to possess unique catalytic properties, presumably a result of the redox properties of V and the acidic character of the molybdophosphoric acid[6]. Interestingly, it is reported that the employment of transition metals oxides (VOx and MoOx) can promote CO oxidation[7], and $H_5PMo_{10}V_2O_{40}$ contains these oxides. It also was discovered that the $H_5PMo_{10}V_2O_{40}$ deposited Pt/C catalysts showed excellent catalytic activity and stability[8]. Taking in account this features, in the present work we synthetized and analysed three different POMs with different amounts of Cs ($Cs_xH_{5-x}PMo_{10}V_2O_{40}$). In order to further understand the promotion effect of POMs on Pt catalyst, POMs modified platinum electrode was studied in real Fuel Cell. The reduction of Platinum loading until 0.125mg cm^{-2} maintaining MEA performance of 1000 mW cm^{-2}, together with low relative humidity (RH) MEAs operation and the enhance of MEAs lifetime are some of important targets contained in The US Department of Energy (DOE) for 2017 and 2020[9]. Recently, many studies have examined the effects of RH on PEMFC performance[10]. This research includes modelling[10], performance evaluation, flow field design[10], degradation of MEA[11], oxygen reduction reaction (ORR)[12], and so on. The results indicate that RH reduction can strongly influence fuel cell performance[13], by increasing the membrane resistance, decreasing the proton activity in catalyst layers, decreasing the Pt utilization, reducing the electrode kinetics, and increasing the gas mass transfer resistance[14]. Our results show that even in a PEMFC operated at 17% of RH, using POMs modified platinum electrode good performance are obtained. Preliminary morphological and electrochemical analysis data are also presented.

2. Experimental

2.1 POM's salt synthesis

Three different salts ($Cs_{2.5}H_{2.5}PMo_{10}V_2O_{40}\cdot 8H_2O$, $Cs_3H_2PMo_{10}V_2O_{40}\cdot 8H_2O$ and $Cs_{3.5}H_{1.5}PMo_{10}V_2O_{40}\cdot 8H_2O$) were prepared using the following procedure. An aqueous solution of Cs_2CO_3 was added drop-wise to the PVM ($H_5PMo_{10}V_2O_{40}\cdot 8H_2O$) solution (in u.p. water) at 50°C under vigorous stirring. The fine suspension was held under stirring at 50ºC for 1h and the stir was maintained overnight at r.t. Subsequently the mixture is filtered with a under vacuum filter system using a hydrophilic filter. The final product was dried overnight in oven at 50°C. The ratio PVM–cesium carbonate was regulated in order to obtain the desired stoichiometry.

2.2 Catalytic layer preparation

The procedure for catalytic layer preparation was to mix in a vial an amount of POM salt with Pt/Vulcan and 985 µl of isopropanol. The mixture was sonicated for 10 seconds in a water bath and for 30 min with ultrasonic processor in ice bath. Only after, 15 µl of Nafion solution were added and the new mixture was put under stirring for 30 min. The weights of salt and Pt/Vulcan are calculated in according to the Pt loading (L_{Pt}) wanted on the electrode. In this thesis usually 10/15 µg Pt/cm^2 are deposited on electrode surface. The Pt/POM/pure Nafion 1:1:1 mass ratio is used. An amount of 4 µl of the prepared ink is deposited on the electrode surface trough a Hamilton 701n 10 µl syringe and let dry for 30 minutes in air.

2.3 MEA preparation

The inks are prepared by following the same procedure reported in *Section 2.2*. For Fuel Cell analysis inks with mass ratio Pt/C : POM : pure Nafion of 2:1:1 are prepared. Pt loading is typically 0.2 mg/cm^2 for modified cathode The slurry was brushed on the gas diffusion layer (GDL) as uniformly as possible to obtain a homogenous thickness on electrode surface. Pt loading on electrode surface was 0.2 mg/cm^2. Nafion synthesized membrane was pre-treated with H_2O_2 and H_2SO_4 to remove organic and inorganic impurities[15]. The MEA was prepared by sandwiching two different synthesized membrane between anode (commercial ETEK, L_{Pt}: 0.5mg/cm^2) and modified cathode. The system was hot-pressed at T = 120 °C for 3 minutes and 50 bar of pressure. Feed gas cell temperature are conventionally specified as TA/TM/TC. TA and TC are anode and cathode feed gas temperatures, respectively, while TM is cell temperature (°C). All the chemicals were used as obtained without further purification. Solutions were prepared using Millipore Milli-Q water of resistivity ≈ 17 MΩ·cm.

2.4 Apparatus

SEM experiments were performed with Leo 1430 (Zeiss). The XRD spectra were recorded on sample powders. X-ray diffraction (XRD) data were recorded using an automated diffractometer equipped by; HV power supply Italstructures, X-ray lamp Philips with Mo anode and CPS180 position sensitive detector with a gas mixture of Kr / CO_2. Divergence of the beam controlled by fissures + soller slits of Huber. The IR spectra of our samples were recorded in the ATR mode (Attenuated Total Reflectance), with PerkinElmer Spectrum 100 Series FT-IR spectrometer. Electrochemical experiments were carried out with the CH Instruments (Austin, TX) model 832, in a Pine AKCELL3 three-electrode cell. The working electrode (RRDE) was a PINE special MT29 series tips with Glassy carbon Rings (collection efficiency: 37%; disk area: 0.2475 cm^2) driven by a Pine rotator 636 ring-disk electrode system (Pine Instruments, USA). The reference electrode was K_2SO_4 saturated Hg/Hg_2SO_4 (SHE), and Pt flag as counter electrode. All the potentials are reported versus the reference hydrogen electrode (SHE). The SHE reference electrode was used to avoid possible contamination of chloride come from electrolyte solution. Two supporting electrolytes of 0.1 M $HClO_4$ and 0.5 M H_2SO_4 in ultra-pure water was used. All electrochemical analysis are made at 25ºC with Haake F3-K Refrigerated Circulating Water Bath. A Fuel Cell of 5 cm^2 area (triple-serpentine cell, model 05-02 from Electrochem. Inc), controlled by a Scribner Associated 890CL fuel cell test system, was used for the fuel cell experiments. For MEA testing pure Hydrogen has been used at anode (100 ml/min) and pure Oxygen at cathode (200 ml/min). The gas pressure was maintained constant at 2 bar. All the potentials are reported

versus the reversible hydrogen electrode (SHE).

3.1 Physicochemical characterization

3. Result and discussion

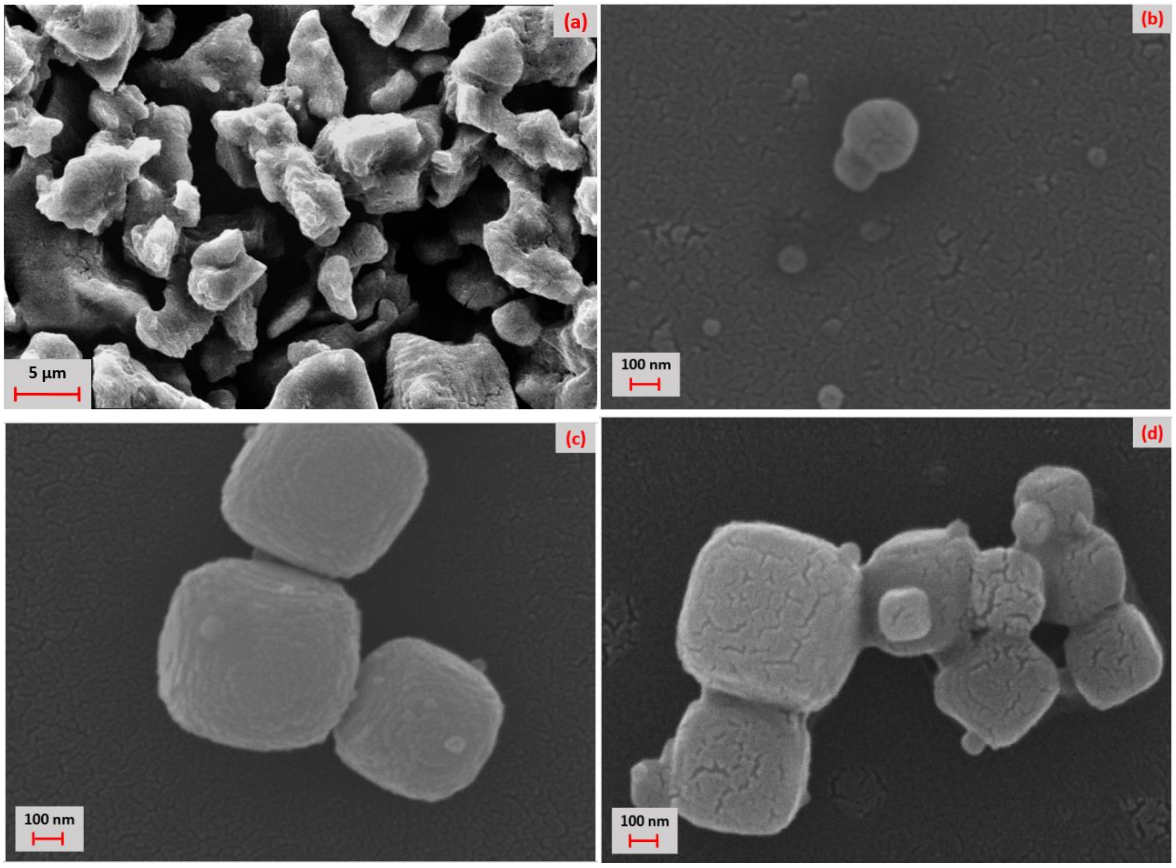

Figure 1: SEM micrographs a) starting HPA; b) POM 2.5-2-10;c) POM

Figure 1 shows SEM micrographs obtained for each POM. POMs presents different type of agglomerates of small cubic nanocrystals grains, that appear to be more dispersed in comparison with the starting HPAs (**Figure 1.a**), which morphology presents different arrays of big crystals (1-10 µm). This confirms a morphological modification as consequence of the Cs introduction during reaction. The POMs grains dimension are included in the range of 50-500 nm. These differences in size are probably in correlation to the higher Cs addition during the synthesis. Moreover, the particles appears closer to cubic morphology increasing the Cs amount.

Figure 2 shows XRD patterns of starting heteropolyacid PVM 2-10 compared with

those of cesium-polyoxometalates.

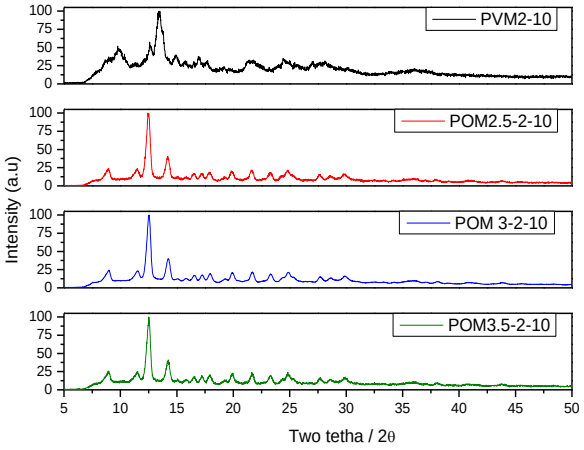

Figure 2: XRD analysis of POM s compared with that of PVM 2-10 (black).

PVM 2-10 exhibits a XRD pattern in agreement with that reported for Keggin-type heteropolyacid[16]. XRD pattern of each POM is very similar to the reference acid, meaning that after the reaction POM salts maintains the Keggin-type structure. Anyway, there are shifts toward lower 2θ values for POMs due the introduction of larger Cs^+ cation**,** into a heteropolyacid compound to replace H^+ will greatly influence its tertiary structure, leading to the formation of micropores and mesopores and the significant increase in specific surface area[17]. Moreover, we can see that peaks for the POMs are more defined than those of the acid, meaning a more ordered crystal lattice.

Figure 3 shows IR spectroscopy comparison between the starting heteropolyacid (PVM 2-10) and the POMs salts. IR spectra of PVM 2-10 shows the characteristic bands of Keggin structure[18], in the region between 800-1200 cm^{-1}. The bands at 741, 858, 955 and 1058 cm^{-1} can be confidently attributed to Mo-O-Mo bridge stretching, Mo = O bond asymmetric stretching and P-O bond stretching of PO_4 tetrahedron. The pattern of the salts is very similar the one of the heteropolyacid but there is a presence of shoulder peak at around 1000 cm^{-1}.

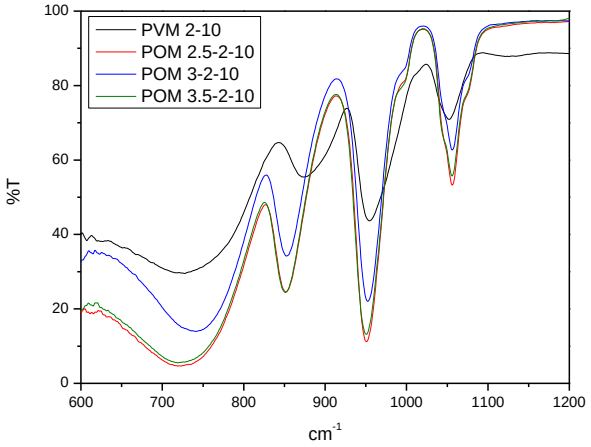

Figure 3: IR spectra of PVM 2-10 (black) and POMs.

Thanks to the presence and distribution of Cs^+ cation in the material, we can see, also in this case, the shift of the IR salts peaks respect to starting PVM.

3.2 Electrochemical characterization with RRDE

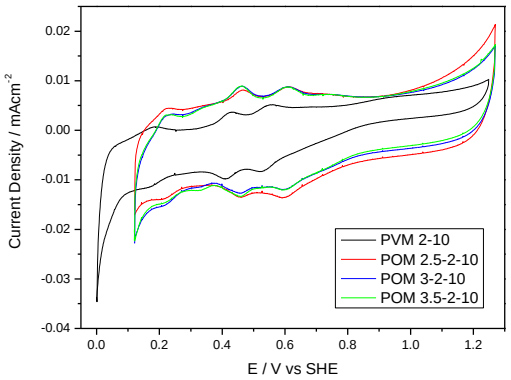

Figure 4: Cyclic voltammetry at GC electrode of PVM 2-10 (black) and Pt-free POMs 2-10 coated electrode. Electrolyte: H_2SO_4 0.5M. Scan rate: 10mV/s.

In **Figure 4** cyclic voltammetry of PVM 2-10 is reported (black). Three redox couples involving Mo^{6+} that undergoes several subsequent reduction step, are observed. The shape is maintained between acid and salts but a shift toward positive potential is observed. According with the literature[19], we can explain

this shift with the presence of the Cs^+ cation in the Kegging structure that goes to affect the thermodynamics of redox processes involved.

In **Figure 5**, Oxygen Reduction Reaction (ORR) for catalytic layers modified with POMs, are reported. We can see a shift of ORR onset potential toward more positive value for modified layers respect to commercial Pt/C 40%. Layers with L_{Pt} = 15 μg/cm^2 for Pt/POMs 2.5-2-10 and 3-2-10 shows, in the first part, a comparable onset potential; while in the final part of the curves is possible to see a higher slope. Higher shift is observed for layers with L_{Pt} = 10 μg/cm^2. These shifts indicates a lower activation energy due to a more favourable kinetics for the ORR. This suggests that the presence of insoluble salt in the INKs improves the catalytic activity of the Pt particles. Several factors such as porosity, surface area, Pt particles dispersion, H^+ availability from POM matrix, and amount of conductive agent may improve the catalytic activity. As we can see, reverse situation for Pt/POM 3.5-2-10 layer is obtained. In this case higher shift is observed for the layers with L_{Pt} = 15 μg/cm^2.

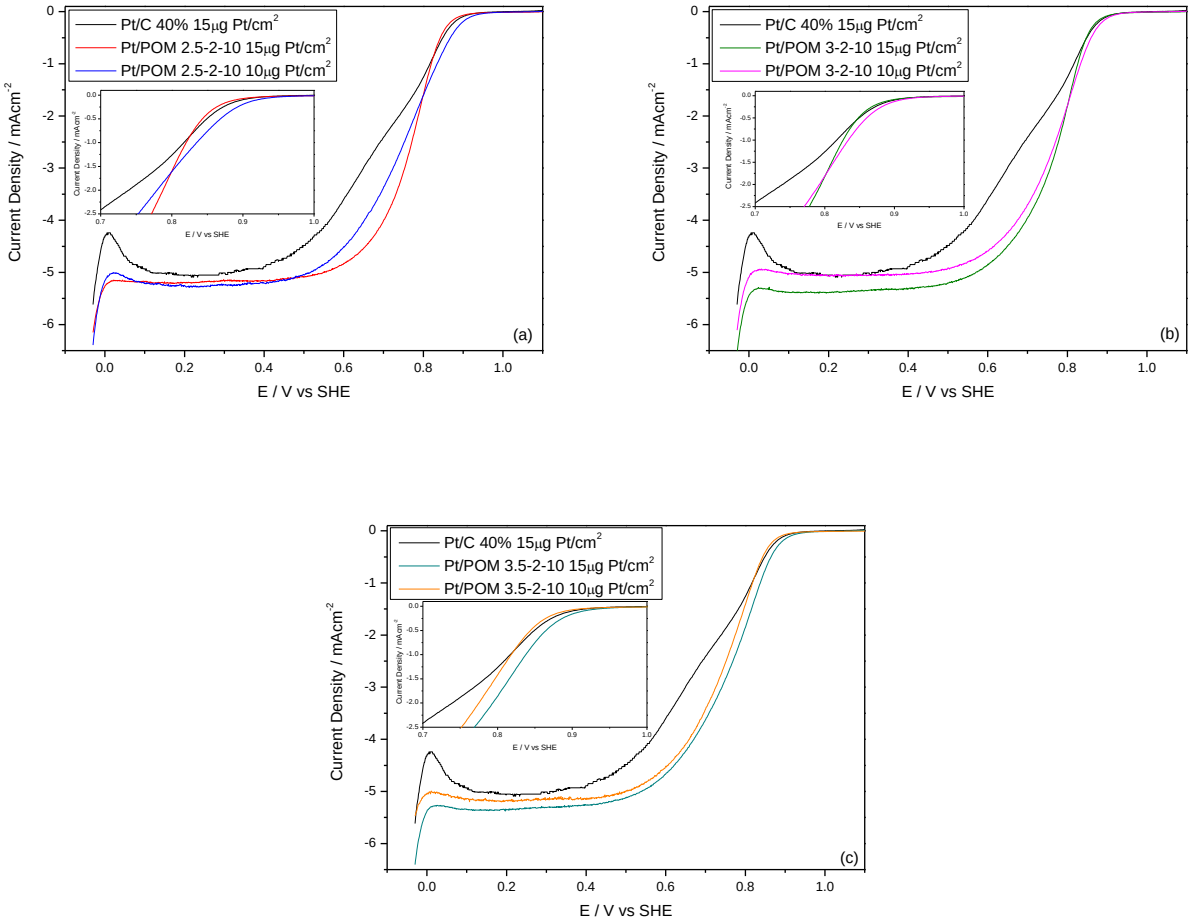

Figure 5: Comparisons of selected RDE voltammograms at 1600 rpm rotation speed for ORR of Pt/C and (a) Pt/POM 2.5-2-10, (b) Pt/POM 3-2-10 and (c) Pt/POM 3.5-2-10 electrodes. Inserts: detail of the onset potential.

From Koutecky-Levich plots (**Figure 6**) is possible to see the dependence of RDE limit current versus square-root of scan rates, as described by the Koutecky-Levich equation:

$$\frac{1}{I} = \frac{1}{I_k} + \frac{1}{I_d} + \frac{1}{I_f} = \frac{1}{I_k} + \frac{1}{C_0 B \omega^{1/2}} + \frac{L}{nFc_f D_f}$$

$$B = 0.62nF{D_0}^{2/3}\upsilon^{-1/6}$$

$$I_k = nFkC_0$$

were I is the experimentally measured current (A), I_k is the kinetic current, I_d is the diffusion-limited current, I_f is inversely proportional of the diffusion resistance through surface film (Nafion), n is the number of electrons transferred in the half reaction (mol^{-1}), F is the Faraday constant (96485 C/mol), A is the electrode area (cm^2), D_0 is the diffusion coefficient of the gas ($1.67 \cdot 10^{-5}$ cm^2/s for O_2), k is the heterogeneous electron-transfer rate constant, ω is the angular rotation rate of the electrode (rad/s), υ is the kinematic viscosity of electrolyte (0.0107 cm^2/s), C_0 is the analyte concentration in the solution ($1.38 \cdot 10^{-6}$ mol/cm^3 for O_2), L is the film thickness, c_f is the reactant concentration in the Nafion film and D_f is the diffusion constant in the Nafion film.

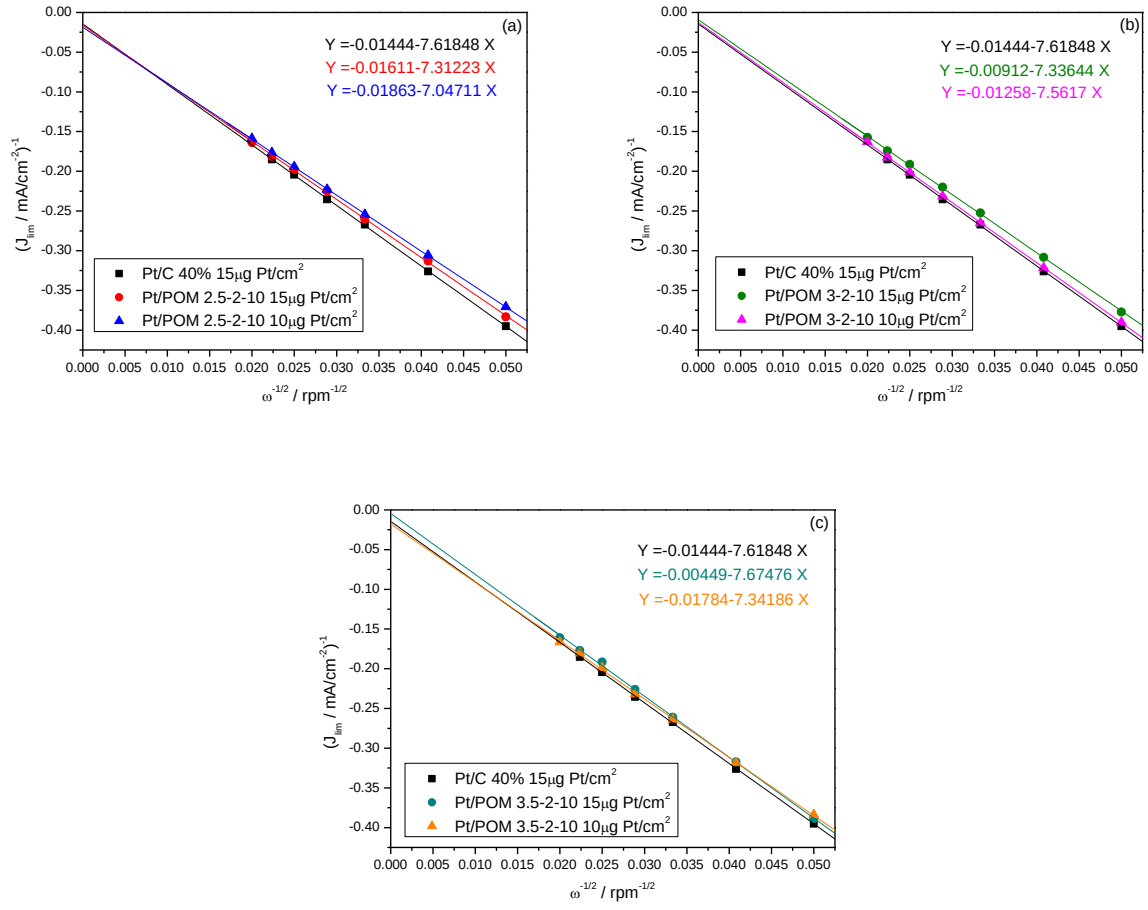

Figure 6: Comparisons of Koutecky-Levich graphs of analysed catalytic layers, obtained using the data in Figure 5 take at 0.3V.

The decrease of K-L plot slope means a more favourable process in the electron exchange and higher reactivity. The K-L plots for all layers are linear with a non-zero intercept as expected for a kinetically limited process, so we can assert that the kinetics limitation are not originated from slow charge propagation or slow diffusion of Oxygen through the catalytic film; in this case they would result into non-linearity[20].

INK	L_{Pt}	Number of electron	BC_o mA·cm^{-2}·rpm$^{-(1/2)}$
Pt/C 40% Alfa Aesar	15 µg Pt/cm2	3.53	0.131
Pt/C 40% + POM 2.5-2-10	10 µg Pt/cm^2	3.81	0.142
Pt/C 40% + POM 3-2-10	10 µg Pt/cm2	3.75	0.140
Pt/C 40% + POM3.5-2-10	10 µg Pt/cm^2	3.66	0.136

Table 1: Comparison between calculate number of electron and BC0 for ORR.

All the BC_o values (**Table 1)** are close to the theoretical one (0.143 mA·cm^{-2}·rpm$^{-(1/2)}$)[21], but the BC_o for Pt/POMs layers appears to be higher than Pt/C value; this means that the process is advantaged for the layer modified with POMs, which produced a best charge transfer, reflecting a probable decrease of rate constant at less negative potential[22].The general decrease of the BC_o compared with the theoretical one is due to the H_2O_2 production typical for this process[2].

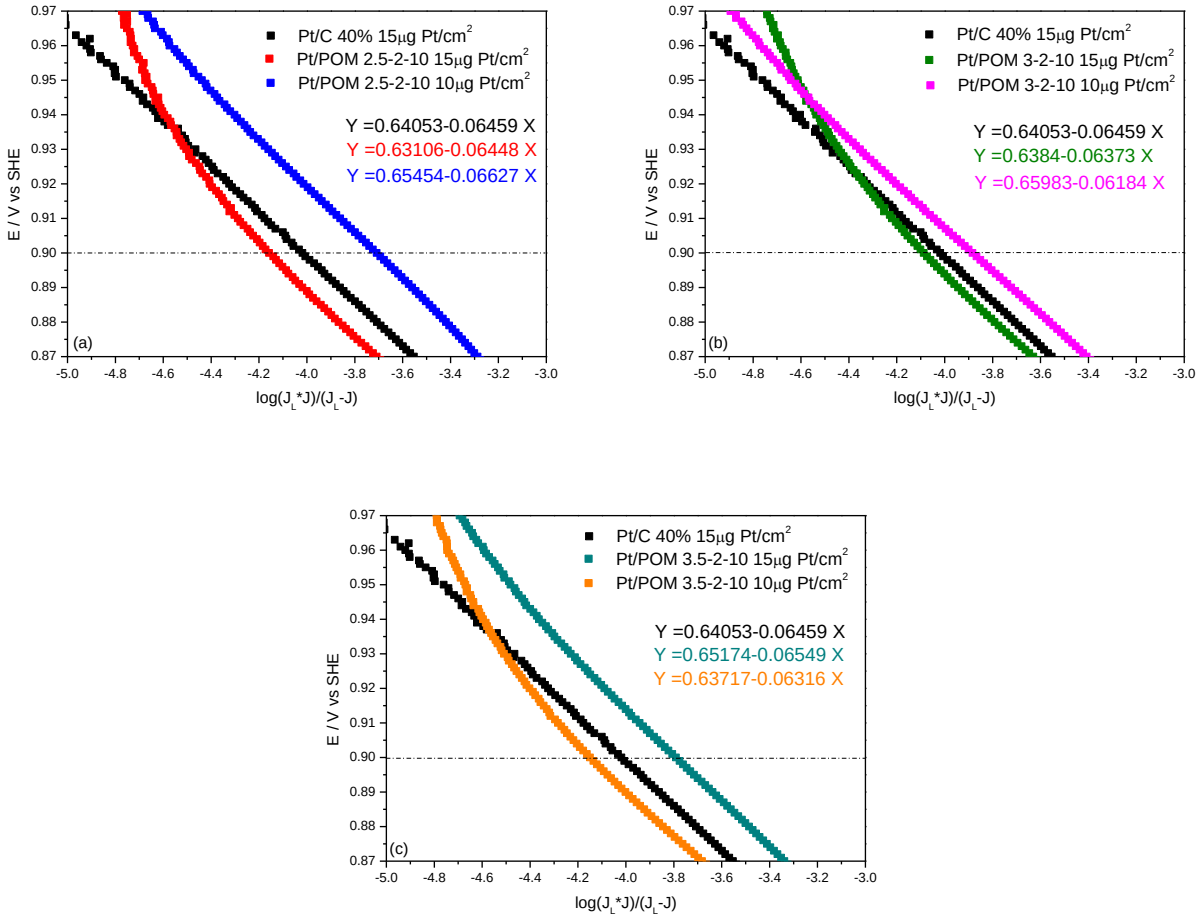

Figure 7: Low overpotential region oxygen Tafel plots at 1600 rpm rotation speed regards the positive going scan of RDE voltammograms.

Figure 7 shows the Tafel plots for different electrodes in the low potential region (0.9 V), where the influence of mass transport is negligible[2]. A good electrochemical speed reaction for layers Pt/POMs 2.5-2-10 and 3-2-10 L_{Pt} = 10 µg/cm^2 and Pt/POM 3.5-2-10 L_{Pt} =

15 μg/cm^2 are confirmed, but layer Pt/POMs 2.5-2-10 and 3-2-10 L_{Pt} = 15 μg/cm^2 and Pt/POM 3.5-2-10 L_{Pt} = 10 μg/cm^2 presents worse performances compared with the unmodified layer. The decrease in performance may be explained by a non-optimal Pt/POM ratio, and by the increase of the layer thickness that disadvantage physically kinetics of the reaction. For layer Pt/POM 3.5-2-10 L_{Pt} = 10 μg/cm^2 the non-good onset potential kinetic is probably due to the slightly high amount of peroxides products during the reaction compared with the other layers with the same L_{Pt}. Anyway, some uncertainties in the results are given by the site-blocking and electronic effect of OH_{ads}[23]. It has been reported by Koper[24] that OH intermediates are formed through dissociative adsorption of molecular oxygen, followed by protonation and via water oxidation. As a consequence, the high amount of OH_{ads} species on Pt surface has an inhibition effect of Pt sites, resulting in reduced ORR rate.

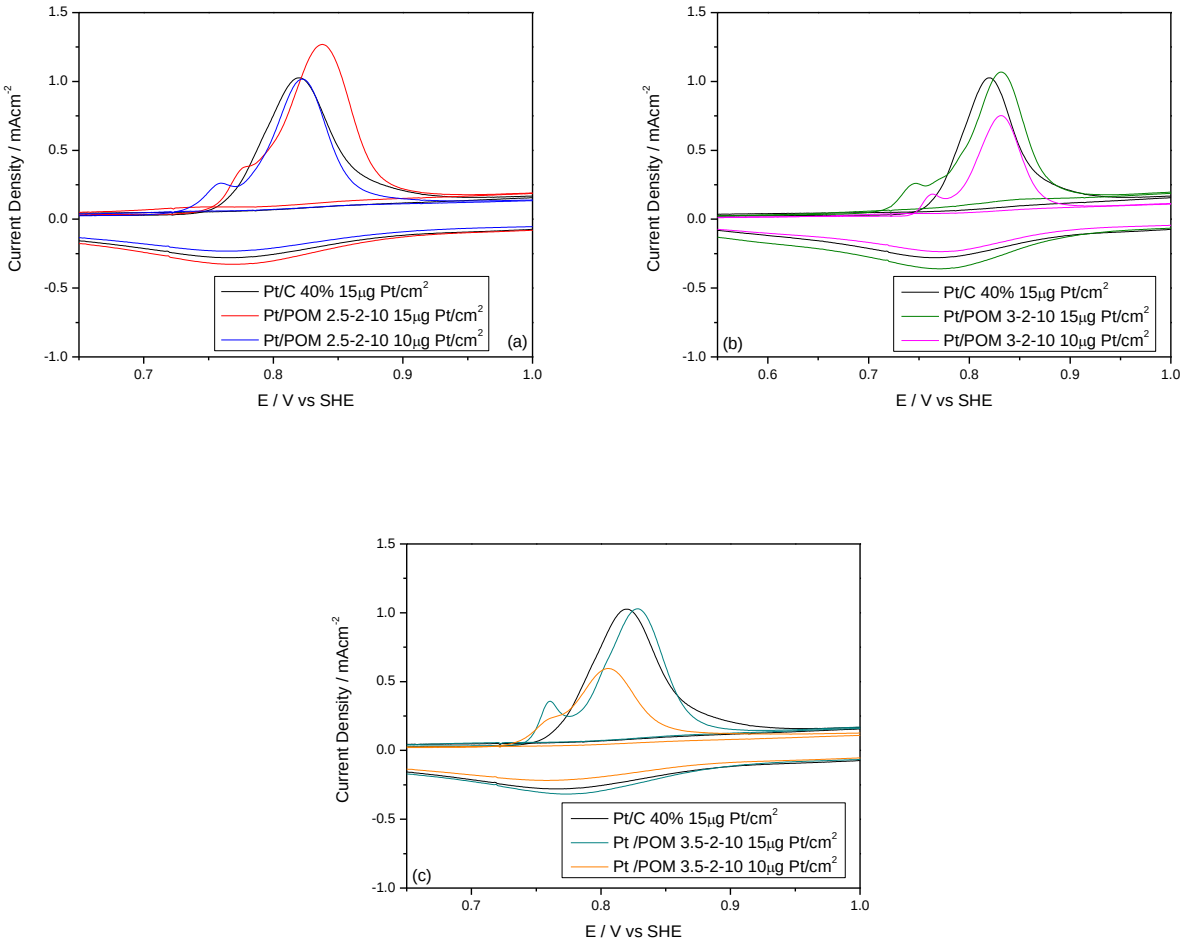

Figure 8: Details of CO stripping voltammetry peaks between 0.6V and 1V vs RHE. Electrolyte: $HClO_4$ 0.1M. Scan rate: 20 mV/s.

In **Figure 8**, details of CO stripping voltammetry peaks between 0.6V and 1V vs SHE, are reported. The Onset potential values of the systems modified with POMs are lower than reference system; the best improvement is observed, also in this case, for low Pt loading Pt/POMs modified layer. The results suggest that the CO stripping starts before for the system modified with POMs compared with the commercial Pt/C 40%. The Cs-POM salts could behave as redox mediator for the CO-oxidation reaction with the Pt present in the

system[22]. The proposed mechanism probably proceeds via the following reaction[25]:

$$POM + CO + H_2O \rightarrow CO_2 + H_2POM$$

$$H_2POM \rightarrow HPA + 2H^+ + 2e^-$$

The catalytic enhancement of the layer with Cs salts containing HPA as matrix may be due to synergistic effect between Pt and POM.

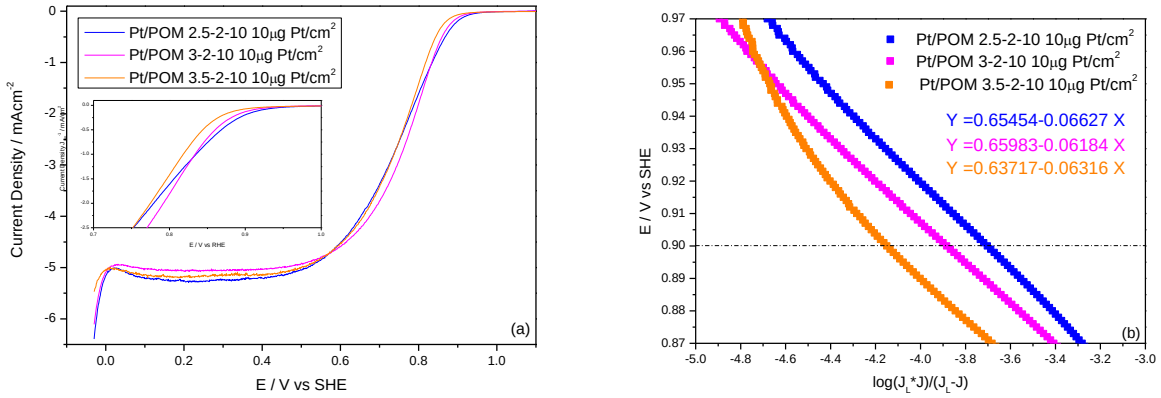

Figure 9: (a) comparison of selected RDE voltammograms for ORR of three Pt/POMs electrodes; (b) low overpotential region oxygen Tafel plots regards the positive going scan of RDE voltammogram for the three Pt/POMs. Rotation speed: 1600 rpm. L_{Pt}: 10 μg/cm^2.

As we have seen from physical analysis, the three POMs presents almost the same characteristics in morphology and structure; from SEM analysis is evident that when the Cs ratio increase, a more defined cubic conformation is observed. After Cs introduction, the co-catalyst results to be better dispersed respect to initial acid, and Keggin-type structure of the starting HPA is maintained after the synthesis reaction. Cubic nanocrystal agglomerates, from 50 nm to 500 nm of size, are formed.

As regards electrochemical analysis, we have obtained different electrochemical performance from the three POMs. In fact POM 2.5-2-10 and POM 3-2-10 with L_{Pt} = 10 μg/cm^2 (**Figure 9(a)**) have shown the best increases in performance compared with unmodified layer with higher Pt loading (15 μg/cm^2). These are very good result, meaning that with decrease in Pt loading, in the case of Pt/POM layers, we can obtain an increase in performance. Tafel Plot analysis in the low overpotential region confirm the good electrochemical speed reaction for layer POM 2.5-2-10 and POM 3-2-10. Worst result is obtained for POM 3.5-2-10 (**Figure 9(b)**). Reverse situation is obtained in the case of POM 3.5-2-10, with which best increase is obtained from the layer with equal Pt loading (15 μg/cm^2) compared with unmodified Pt/C.

Taking into consideration these results, we decided to analyse POMs 2.5-2-10 and 3-2-10 in working fuel cell, because they have shown improvements in performance with the low Pt content, which is one of the main goals of this work.

3.3 Electrochemical characterization in Fuel Cell.

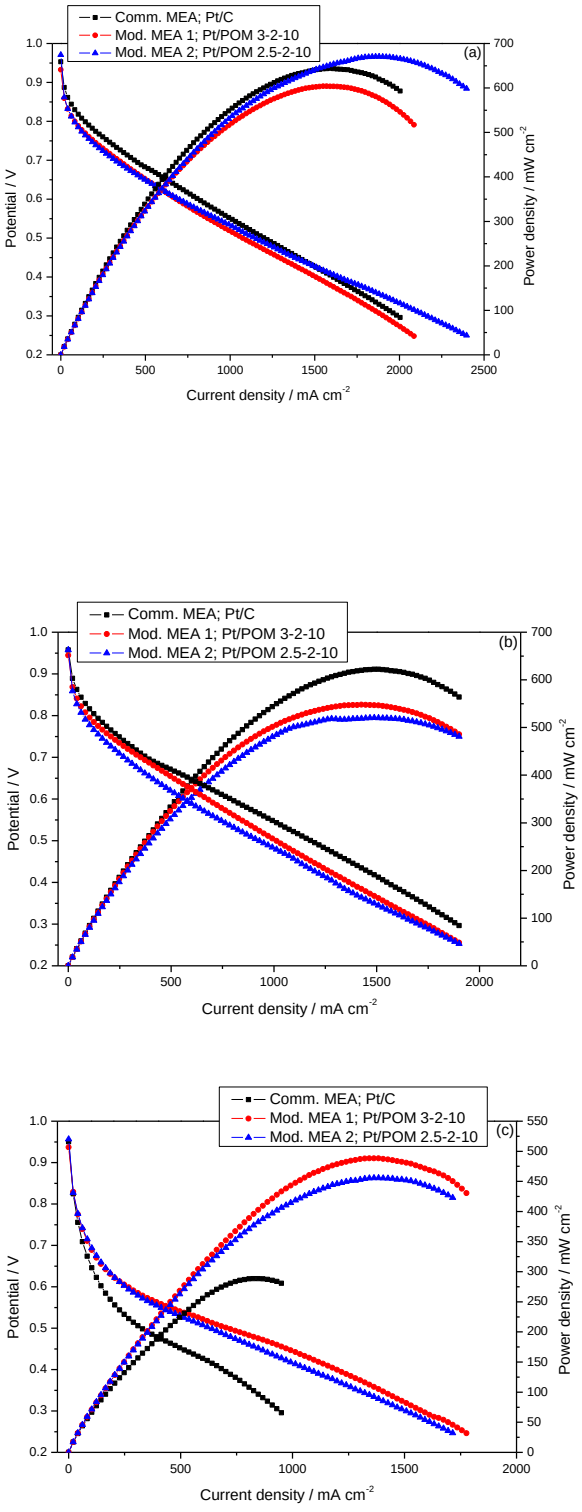

Figure 10: Polarization and power curves of: Comm. MEA (black); Mod. MEA 1 (red); Mod. MEA 2 (blue), obtained with (a) 100% RH (70/70/70); (b) 62% RH (60/70/60); (c) 17% RH (40/70/40) feed gas: H_2 100ml/min, O_2 200ml/min; pressure: 2 bar.

Results obtained with a Fuel Cell employing a MEA made of commercial electrodes and separator are compared with modified MEA employing Pt/POM 2.5-2-10 and Pt/POM 3-2-10 cathodes(**Figure 10**). For each MEA, the anode is always a commercial ETEK (L_{Pt}: 0.5 mg/cm^2) and cathode is prepared using Pt/POMs ($L_{Pt} \approx 0.2$ mg/cm^2) over commercial gas diffusion layer (GDL). We analysed three different MEAs:

Comm. MEA = anode: Pt/C ETEK 0.5 mg/cm^2; cathode: Pt/C ETEK 0.5 mg/cm^2;

Mod. MEA 1 = anode: Pt/C ETEK 0.5 mg/cm^2; cathode: Pt/POM 3-2-10 0.198 mg/cm^2;

Mod. MEA 2 = anode: Pt/C ETEK 0.5 mg/cm^2; cathode: Pt-POM 2.5-2-10 0.21 mg/cm^2;

Figure 10 shows performance tests performed at 100%, 62% and 17% relative humidity. Despite the very low Pt loading at the cathode Mod. MEAs (62% reduction of Pt mass content), in the cases at 100% RH and 62% RH, the performances are only slightly reduced. Differences between the two Mod. MEAs may be explained by a possible cell flooding during the analysis, or possible uncertainties and errors during inks preparation or cell assembly. In fact, at 17% RH, an outstanding improvement of catalytic activity of the Pt nanoparticles supported by insoluble POMs respect to the commercial electrodes is observed, confirming the possible cell flooding in the previous experiments. Therefore, it's possible to confirm that the lower Pt loading is compensated by the higher Pt active surface and better charge transfer respect to commercial MEA, because of the same concurrent enhancing effects, already evidenced in previous RRDE characterization, as improved porosity and surface area, H^+ availability from acid POM matrix, improved Pt particles dispersion.

AC impedance spectroscopy measurements are performed in order to have a better comparison, on the electrochemical behavior,

between commercial MEA and modifies MEAs. The impedance are collected at potentials of 0.4 V and 0.8 V, allowing the understanding of behavior at high and low current densities, respectively.

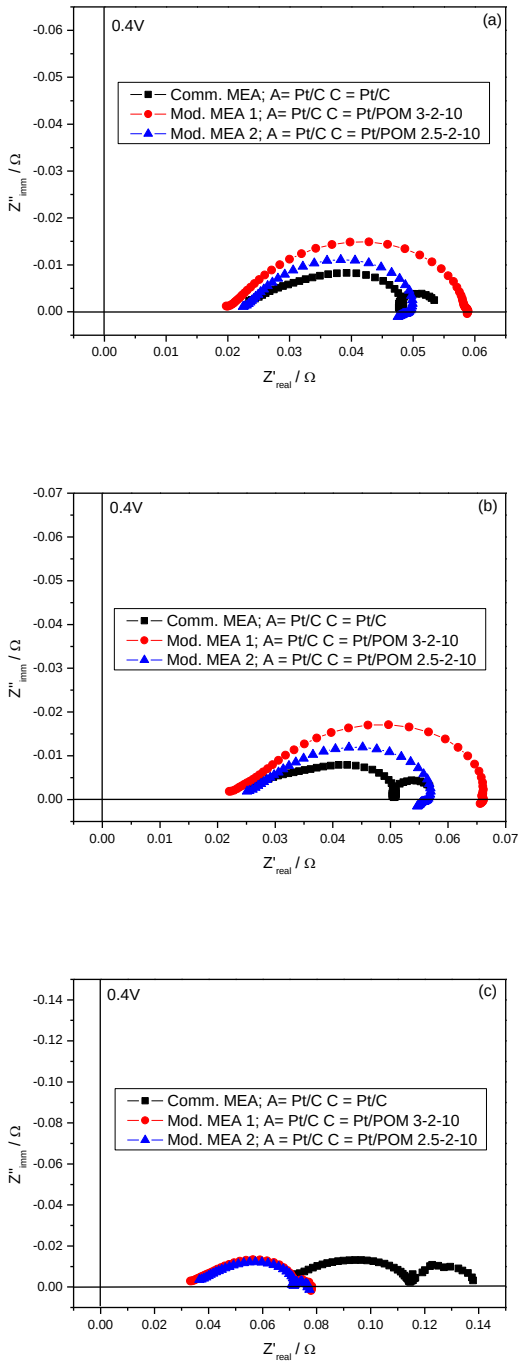

Figure 11: Nyquist plot of impedance spectroscopy tests of Comm. MEA and Mod. MEAs at 0.4V obtained with: (a) 100% RH (70/70/70); (b) 62% RH (60/70/60); (c) 17% RH (40/70/40).

Impedance results at high current densities (0.4 V) show that electrolyte resistance values (R_{el}) for all experiment are comparable; Mod. MEA 1 shows a slightly lower value in all RH conditions. In 100% and 62 % RH conditions, the first high frequency arc (R_{ct}) is visible for both experiments (combination of charge transfer resistance for the ORR and double layer capacitance within the catalyst layer) and shows higher values only for Mod. MEA 1 and comparable value for Mod. MEA 2, respect to Commercial reference, confirming the results obtained in polarization curves. The second arc at low frequency is visible only for Comm. MEA, and is associated with the mass-transport limitations of gas phase reactant (Oxygen), within the gas diffusion media. This is not visible for Mod. MEAs, hence no present limitation in mass-transport, meaning a more favourable transport of reactant, thanks to high porosity of POMs used. The results of Impedance spectroscopy at RH 17% highlight the good results obtained with POMs use to build cathode. As is possible to see in **Figure 11(c)**, using the same polymer electrolyte membrane, the electrolyte resistance (R_{el}) undergoes a sharp drop, emphasizing that the high acidity of POM-based cathodes brings to higher H^+ availability, reducing resistance of proton transfer through the membrane. Also resistance to the charge transfer (R_{ct}) is lower, which means a favourable kinetics using POMs matrix as co-catalysts.

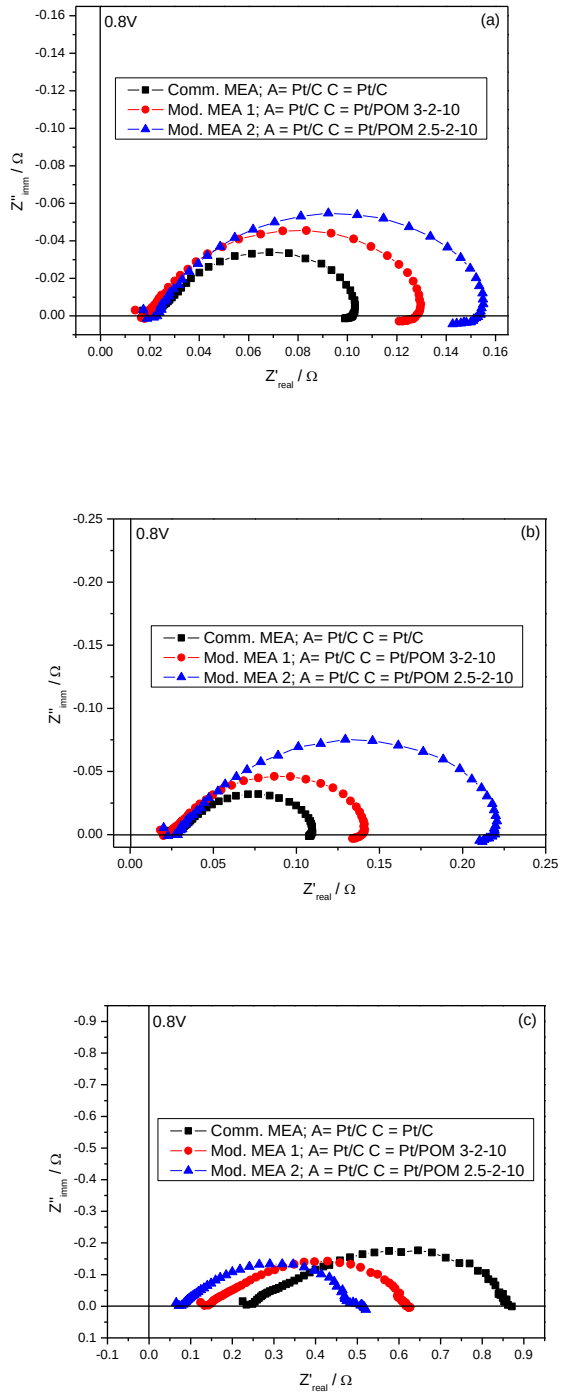

Figure 12: Nyquist plot of impedance spectroscopy tests of Comm. MEA and Mod. MEAs at 0.4V obtained with: (a) 100% RH (70/70/70); (b) 62% RH (60/70/60); (c) 17% RH (40/70/40).

Figure 12 shows results obtained for impedance analysis at low current density (0.8 V). At RH 100% and 62% R_{el} values are comparable, while R_{ct} resistance for both Mod MEAs shows higher values respect to Comm. MEA, as expected. At Rh 17% (**Figure 12(c)**) the results is confirm as well. Both R_{el} and R_{ct} are undergoes decrease confirming the good results obtain at high current density.

The results at high RH are very interesting, because the POMs presence at the cathode compensate the low Pt loading, achieving very good and comparable performance with respect to Comm. MEA; mainly thanks to high POMs acidity that provide high H^+ presence. The slight performance reduction can be attributed to low Pt content and a possible flooding that hides the real efficiency. Reducing RH at 62%, the results are almost the same. We have obtained outstanding results with a further reducing RH until 17%. The cell performance, even with Pt content reduced more than 60%, are greatly increased because POMs seem to act as humidity reservoirs. Both calculated resistances (R_{el} and R_{ct}) decrease, highlighting the improvement of H^+ transfer thorough the membrane and the better kinetics of charge transfer. This is thanks to high dispersion of Pt and enhances of active area, high porosity that reduce the mass-transport limitations of gas phase reactant (Oxygen) within the gas diffusion media and higher H^+ availability due to POM acidity.

4. Conclusion

In order to improve the ORR kinetics involved in PEM-fuel cells, insoluble polyoxometalates with formula $Cs_{2.5}H_{2.5}PMo_{10}V_2O_{40}\cdot 8H_2O$, $Cs_3H_2PMo_{10}V_2O_{40}\cdot 8H_2O$ and $Cs_{3.5}H_{1.5}PMo_{10}V_2O_{40}\cdot 8H_2O$ are synthesized, starting from the corresponding heteropolyacid $H_5PMo_{10}V_2O_{40}$. These salts are first physically an electrochemically characterized, then tested as co-catalysts support for Pt. The presented SEM analysis suggests a morphological modification when, after the synthesis process, protons in heteropolyacid are replaced by Cs^+ cations. In fact starting HPA presents larger

and irregular morphology while POMs salts present smaller and more cubic nanocrystals grains. We can hypothesize that with the increment of the Cesium amount in the structure, this latter appears with a more defined cubic structure. IR spectra performed show that the primary Keggin structure of the HPA remains unaltered when protons are replaced by Cs^+ cations. Good results are obtained from RRDE electrochemical analysis. Investigated material have shown comparable performance at the same Pt loading (15 $\mu g/cm^2$) of the commercial reference and better performance when the L_{Pt} is lowered to 10 $\mu g/cm^2$ for POMs modified systems. There are two hypotheses may be put forward to explain the improvement of the catalytic activity of the Pt supported by POMs to the naked catalyst. One hypothesis regards the increase of the electrochemical properties due to high surface acidity, high proton conductivity, insolubility in water and fast redox behaviour, hence increase the kinetics and catalytic properties. The other hypothesis is oriented on the morphologies of the modified electrodes. Due to peculiar structure of the salts, the Pt nanoparticles trapped in the pores cannot grow above certain dimensions, decreasing the trend of the particles to aggregate and increasing the available active area. Moreover, the introduction of the Cs^+ in the Kegging structure leads to the formation of micropores and mesopores resulting in a significant increase in specific surface area, hence the permeability of the gases. Despite about 60% reduction of Pt mass content, Fuel cell test using Pt/POMs-modified cathodes show comparable performance in RH = 100% and RH = 62% conditions, while better activity are obtained at RH = 17 %. Therefore, the good activity registered with RRDE for Pt/POMs modified electrodes are also confirmed for real Fuel cell system, promising an important reduction of PEM-fuel cells cost and future developments in the use of this type of technology.

Acknowledgments

I would like to thank Dr. Marco Renzi that helped me in the realization of this thesis work and Dr. Francesco Nobili that gave me the opportunity to perform this work. Finally, I thank professor Matilde Marques.

[1] K.R. Cooper, V. Ramani, J.M. Fenton, H.R. Kunz, *Experimental Methods and Data Analyses for Polymer Electrolyte Fuel Cells,* **(2005)**.

[2] S.Dsoke, A. Kolary-Zurowska, A. Zurowski, P. Mignini, *J. of Power Sources*, 196 **(2011)** 10591-10600.

[3] A.S Aricò, S. Srinivasan, V. Antonucci, *DMFCs: From Fundamental Aspects to Technology Development*, *Fuel Cells* 1 **(2001)** 133.

[4] J. Fournier, G. Faubert, J.Y. Tilquin, R. Cote, D. Guay, J.P. Dodelet, *J. Electrochem. Soc,* 144 **(1997)** 145.

[5] P. Gouzerh, M. Che, *L'actualité Chimique*, 298 **(2006)** 9.

[6] Zhiming Cuia, Wei Xinga, Changpeng Liua, Dan Tianb, Hong Zhangb, *J. of Power Sources*, 195 **(2010)** 1619–1623.

[7] M.V. Martínez-Huerta, J.L. Rodríguez, N.Tsiouvaras, M.A. Pe˜na, J.L.G. Fierro, E. Pastor, *Chem. Mater*, 20 **(2008)** 4249.

[8] Ligang Feng, Qing Lv, Xiujuan Sun, Shikui Yao, Changpeng Liu, Wei Xing, *J. of Electronal. Chem.*, 664 **(2012)** 14–19.

[9] DOE, Hydrogen, Fuel Cell and Infrastructure Technologies Program Multiyear Research, Development and Demonstration Plan, Department of Energy, US, **(2011)**.

[10] W. Sugimoto, K. Aoyama, T. Kawaguchi, Y. Murakami, Y. Takasu, *J. Electroanal. Chem*., 576 **(2005)** 215–221.

[11] B.P. Hahn, K.J. Stevenson, *Electrochim. Acta*, 55 **(2010)** 6917–6925.

[12]K.C. Neyerlin, H.A. Gasteiger, C.K. Mittelsteadt, J. Jorne, W. Gu, J., *Electrochem. Soc.*, 152 **(2005)** A1073.

[13]Jianlu Zhang, Yanghua Tang, Chaojie Song, Zetao Xia, Hui Li, HaijiangWang, Jiujun Zhang, *Electrochim. Acta*, 53 **(2008)** 5315–5321.

[14] R. Jiang, H. Russell Kunz, J.M. Fenton, *Electrochim. Acta*, 51 **(2006)** 5596.

[15] Yaliang Tang, Anette M. Karlsson, Michael H. Santare, Michael Gilbert, Simon Cleghorn, William B. Johnson, *Materials Science and Engineering A*, 425 **(2006)** 297–304.

[16] M. Langpape, J.M.M Millet, U.S. Ozkan, M. Boudeulle, *J. Catalysis*, 181 **(1999)** 80.

[17] M. Sun, J. Zhang, C. Cao, Q. Zhang, Y. Wang, H. Wan, *Applied Catalysis A : General*, 349 **(2008)** 212-221.

[18] J.K. Lee et al., *Applied Catalysis A: General*; 214 **(2001)** 125.

[19] M. Ai, *Appl. Catal*., 4 **(1982)** 245.

[20] C.P. Andrieux, J.M. Dumas-Bouchiat, J.M. Saveant, *Journal of Electroanalytical Chemistry*, 131 **(1982)** 1.

[21] U. A. Paulus et al., *J. Phys. Chem. B*, 16 (**2002)** 106.

[22] M. Chojak, A. Kolary-Zurowska, R. Wlodarczyk, K. Miecznikowski, K. Karnicka, B. Palys, R. Marassi, P. J. Kulesza, *Electrochimica Acta* 52, **(2007)**, 5574–5581.

[23] J. X. Wang, N.M. Markovic, R. R. Adzic, *J. Phys. Chem. B*, 108 **(2004)** 4127-4133.

[24] Marc T.M. Koper, *Fuel cell catalysis a surface science approach*, **(2009)**.

[25] R.J. Santis, M.-C. Kuo, J.A. Turner, A.M. Herring, *J. Electrochem. Soc.*, 155 **(2008)** B155.